

Microstructural evolution mechanism and mechanical properties of FeNiCrAl alloy with coherent NiAl strengthening via thermite synthesis: Postprint

Authors: Wang Xing, Xi Wenjun, Cui Yue, Li Shujie

Date: 2023-03-19T00:00:00+00:00

Abstract

The microstructure of FeNiCrAl alloys prepared by aluminothermic synthesis was investigated using XRD, SEM, TEM, and other experimental methods, and the effect of Al content in the thermite composition on the tensile properties of the alloys was studied. The results show that when the Al content in the thermite is no more than 25.4% (mass fraction), the main constituent phase of the alloy is austenite; when the Al content in the thermite reaches 26.6%, the main constituent phase of the alloy is ferrite, and a granular NiAl phase precipitates; as the Al content continues to increase, the granular precipitate phase is gradually replaced by a woven-like structure. The formation of the woven-like structure is the result of liquid-phase spinodal decomposition. The increase of Al content in the thermite reduces the elongation after fracture of the alloy. When the Al content in the thermite is 26.6%, the tensile strength of the alloy reaches its maximum value of 640.87 MPa.

Full Text

Microstructure Evolution Mechanism and Mechanical Properties of NiAl-Coherently-Strengthened FeNiCrAl Alloys Synthesized by Thermite Process

WANG Xing, XI Wenjun, CUI Yue, LI Shujie

School of Materials Science and Engineering, Beihang University, Beijing 100191

Correspondent: XI Wenjun, professor, Tel: (010)82338190, E-mail: xiwj@buaa.edu.cn

Supported by National Natural Science Foundation of China (No.51472015)

Manuscript received 2014-09-09, in revised form 2014-12-09

Abstract

The excellent thermal conductivity, low thermal expansion coefficient, and high oxidation resistance of ferritic FeNiCrAl alloys provide them with the potential to replace nickel-based superalloys in high-temperature applications. However, their usage is limited by poor high-temperature mechanical properties. The high melting point of NiAl intermetallic compounds, together with their excellent high-temperature stability and similar lattice parameters to α -Fe, allows them to coherently strengthen ferritic FeNiCrAl alloys and extend their high-temperature performance. Traditionally, these Fe(Ni, Cr)/NiAl alloys are prepared by vacuum reaction melting followed by an aging process. However, the aging process has drawbacks including excessive cost, lengthy processing times, and coarsening of the NiAl phase at elevated temperatures. A more cost-effective thermite reaction process was explored to prepare Fe(Ni, Cr)/NiAl alloys. In this approach, ferritic FeNiCrAl alloys were strengthened by a high volume fraction of nanoscale NiAl phase achieved without requiring an aging process.

Several types of thermite compositions were designed and studied to explore the transformations of alloy microstructures and changes in tensile properties with varying thermite compositions. The microstructures of these thermite-synthesized Fe(Ni, Cr)/NiAl alloys were investigated using XRD, SEM, EDS, TEM, and SAED. The effect of Al content in the thermites on alloy microstructures was examined. Experimental results showed that when the thermites contained no more than 25.4% (mass fraction) Al, the synthesized Fe(Ni, Cr)/NiAl alloys were composed primarily of an austenite phase. When the mass fraction of Al in the thermites reached 26.6%, the main component phase of the alloy transformed into ferrite, while NiAl particle precipitates emerged. As the Al content in the mixture was further increased, the NiAl precipitates were gradually replaced by an intertexture structure. The intertexture structure became completely dominant when the mass fraction of Al in the thermites reached 31.4%. This microstructure consisted of a ferritic FeNiCrAl matrix with a width of 80–100 nm and NiAl precipitates with a width of about 50 nm, with the two phases maintaining coherent matching. This microstructure resulted from liquid spinodal decomposition. The effect of Al content on mechanical properties was also investigated. Increasing Al content in the thermites decreased alloy elongation, which varied from 25.5% to 1.7% when the mass fraction of Al ranged from 24.2% to 29.0%. When the thermites contained 26.6% mass fraction Al, the tensile strength of the alloy achieved its maximum value of 640.87 MPa.

KEY WORDS thermite process, NiAl, tensile property, liquid spinodal decomposition

Introduction

Compared with heat-resistant austenitic steels, heat-resistant ferritic steels offer advantages including low thermal expansion coefficient, excellent high-temperature oxidation resistance, high thermal conductivity, good radiation damage resistance, and low cost, making them promising for applications in the nuclear industry and future fusion reactors. However, their high-temperature strength and creep resistance above 600 °C are relatively poor, limiting their application range [1]. Research [2] has shown that the high-temperature creep resistance of ferritic alloys can be effectively improved through coherent two-phase strengthening mechanisms. The B2-structured NiAl intermetallic compound has a bcc structure like α -Fe, and its lattice constant (0.28864 nm) is very close to that of α -Fe (0.28665 nm) [3], thus satisfying the requirements for serving as a coherent strengthening phase in bcc iron-based alloys and producing a γ - γ' coherent strengthening structure similar to that in nickel-based superalloys [4,5].

Currently, the preparation of coherently precipitation-strengthened Fe-Ni-Al alloy systems is mainly achieved through vacuum reaction melting and aging. Calderon et al. [2,6] conducted extensive studies on the aging behavior of Fe-Ni-Al alloys at different temperatures and times, and discussed the coarsening kinetics of the system. To improve the oxidation resistance of the alloy system, Hao et al. [7] added Cr to the Fe-Ni-Al system and found that Cr almost completely dissolved in α -Fe. Fe-Ni-Cr-Al alloys combine the excellent oxidation resistance of ferritic Fe-Cr-Al alloys with the superior high-temperature strength of Fe-Ni-Al alloys containing high volume fractions of the B2 phase, and have potential as a new type of high-performance high-temperature structural material through precipitation of the NiAl ordered phase in the iron matrix [8]. Vo et al. [9] thoroughly investigated the microstructure of aged Fe-Ni-Cr-Al alloys, statistically analyzed the volume fraction and size of NiAl precipitates in α -Fe, and studied microstructural and property changes after high-temperature creep.

Bradley and Taylor [10], through phase diagram and thermodynamic studies of the system, concluded that with sufficient Al, the volume fraction of NiAl precipitates in α -Fe could vary over a wide range. Stallybrass and Sauthoff [8] aged Fe-Ni-Cr-Al alloy samples at 900 °C for 100 h and found that as the Al and Ni content in the raw materials increased, the NiAl precipitates not only increased in volume fraction but also gradually changed from a particle shape to a previously unobserved intertexture structure. They studied the compressive yield strength of this alloy at high temperature but did not explain the formation mechanism of this intertexture structure.

The method of preparing NiAl-coherently-strengthened Fe-Ni-Cr-Al alloys through aging still suffers from problems such as excessively long cycles, high production costs, and coarsening of the NiAl phase during prolonged high-temperature aging. Therefore, researchers continue to explore new prepa-

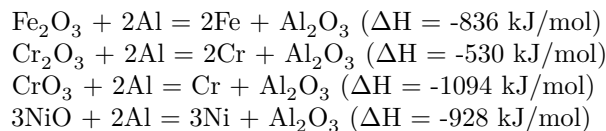
ration methods for Fe-Ni-Cr-Al alloys. Combustion synthesis, as a method for preparing high-temperature, refractory, and wear-resistant materials, has attracted increasing attention from scholars worldwide due to its low cost, energy efficiency, and simple equipment, particularly when combined with traditional processes such as centrifugal casting [11-14]. In this work, Fe-Ni-Cr-Al alloys were prepared through thermite reaction combustion synthesis. This process is simple, has short reaction times, and can produce ferritic alloys strengthened by nanoscale, high-volume-fraction NiAl phases without using an aging process, avoiding the long processing times, high costs, and NiAl phase coarsening associated with aging. By increasing the Al content in the thermite, the intertexture microstructure observed by Stallybrass and Sauthoff [8] through aging also appeared in the samples. This work attempts to discuss the formation mechanism of this intertexture structure and investigate the effects of varying Al content in the thermite on sample microstructure and tensile properties.

1 Experimental Methods

Fe(Ni, Cr)/NiAl alloys were synthesized using a thermite reaction process with Fe_2O_3 , NiO, Cr_2O_3 , CrO_3 , and Al as thermite raw materials. To ensure that the obtained alloys could satisfy the thermodynamic conditions for coexistence of α -Fe and NiAl phases and that the thermite reaction would release sufficient heat for complete reaction, the thermite compositions used in this experiment were designed based on relevant phase diagrams [15] and Thermo-Calc thermodynamic software, as shown in Table 1. The Al content of the reducing agent varied across compositions while other components remained constant. The total mass of thermite used in each experiment was 500 g.

The sample preparation process was as follows: The thermite powder was ground and mixed uniformly, then placed in a graphite crucible (with a small hole at the bottom) sealed with Al foil and wrapped with insulation material to prevent heat loss. The crucible with insulation was placed in a drying oven and held at 120 °C for 2 h before removal. The thermite reaction synthesis setup is shown in Figure 1 [Figure 1: see original paper]. The graphite crucible was placed on a Cu mold with a ceramic filter inserted between them to filter out impurities produced during reaction. The powder was ignited with a heated W wire, and once ignited, the redox reaction proceeded, sustained by the heat released from the reaction.

The chemical reactions during the process are complex, but the main reactions are generally considered to be:



where ΔH represents the heat released per mole of reaction at room temperature.

According to reaction equations (1)-(4), the main reaction products are Fe, Ni, Cr, and Al_2O_3 . The reactions release substantial heat, melting all products. Al_2O_3 has low density and poor wettability with the FeNiCrAl alloy melt, giving it a tendency to separate from the melt under gravity. Due to the extremely high temperatures reached during the thermite reaction, Al_2O_3 has sufficient time to float out of the alloy during melt solidification, forming an Al_2O_3 slag layer. After solidification, macroscopic separation between Al_2O_3 and the alloy is complete, and the upper Al_2O_3 slag layer is removed to obtain the alloy sample.

During the reaction, the high-temperature melt melted through the Al foil and poured into the pre-placed Cu mold. After solidification, the surface Al_2O_3 slag layer was removed to obtain the alloy sample. The resulting alloy samples were cylindrical with a diameter of approximately 16 mm, length of about 120 mm, and mass of about 150 g. The mass loss originated from separation of impurities and material splashing during the reaction.

The microstructures of the alloys were observed using a JSM-6010LA scanning electron microscope (SEM) and an Apolo-300 field-emission SEM. Microstructural morphology and phase compositions were further investigated using a JEM-2100F transmission electron microscope (TEM) combined with selected-area electron diffraction (SAED) and energy-dispersive spectroscopy (EDS). For certain alloy compositions, samples were aged at 500, 700, and 900 °C for 100 min, and their microstructural changes were observed using the JSM-6010LA SEM.

Tensile properties were tested using an MTS810 materials testing machine, and fracture morphologies of tensile specimens were examined with the JSM-6010LA SEM. Alloy samples were machined by wire cutting into tensile specimens with a gauge length of 10 mm, thickness of 1.5 mm, width of 2.5 mm, and total length of 34 mm. To eliminate potential adverse effects of surface defects on mechanical properties, specimens were ground flat and polished to a bright finish. To eliminate machine error during tensile testing, BX120-2AA strain gauges were attached to the samples and connected to a JC-4a intelligent static strain gauge. The curves measured by the strain gauge were fitted with those from the tensile testing machine to obtain accurate stress-strain curves.

2 Results and Discussion

2.1 Effect of Thermite Composition on Microstructure Figure 2 [Figure 2: see original paper] shows SEM images of samples synthesized from thermites with seven different Al contents. Figures 2a and 2b present SEM images of samples synthesized with Al contents of 24.2% and 25.4% in the thermite, respectively. Both alloys consisted of dendrites with grain sizes of 5-10 μm . XRD patterns (Figure 3 [Figure 3: see original paper]) indicated that the alloys were composed of fcc austenite. EDS analysis results (Table 2) showed that the alloys mainly contained Fe, Ni, Cr, and Al at this stage.

Figure 2c shows the SEM image of a sample synthesized with 26.6% Al in the thermite. The alloy consisted of equiaxed grains 40–50 μm in diameter. EDS analysis (Table 3) indicated that the alloy still mainly contained Fe, Ni, Cr, and Al. XRD patterns (Figure 3) showed that when Al content in the thermite exceeded 26.6%, the main constituent phase of the alloy changed from fcc austenite to bcc ferrite. At this point, three major diffraction peaks appeared at $2\theta = 44.50^\circ$, 64.75° , and 81.96° , representing overlapping peaks from bcc ferrite and B2-structured NiAl intermetallic compounds. The crystal structures of ferritic alloy and NiAl intermetallic compounds are essentially the same, and their lattice constants are very similar, so their main peak positions basically coincide.

When Al content in the thermite continued to increase to 27.8%, numerous fine granular precipitates began to appear inside the alloy grains, with fine plate-like structures forming at some grain boundaries (Figure 2d). From the high-magnification SEM image of the intragranular structure (Figure 2e), the granular precipitates appeared cubic with sizes of 50–100 nm. Combined with XRD results, a weak superstructure diffraction peak appeared at $2\theta = 31.06^\circ$, indicating the presence of ordered NiAl phase. It is speculated that the cubic black particles are NiAl intermetallic compounds. Figures 2f and 2g show the microstructures of alloys synthesized with Al contents of 29.0% and 30.2% in the thermite, respectively. As Al content further increased, the plate-like structures that initially appeared only at grain boundaries began to extend into the grains, forming large-area intertexture structures between grains, with some small grains entirely composed of intertexture structures. When Al content in the thermite reached 31.4% (Figures 2h and 2i), the alloy consisted of equiaxed grains 20–30 μm in size permeated by intertexture structures throughout.

Figure 4a [Figure 4: see original paper] shows a TEM image of cubic precipitates inside grains. The precipitates measured 50–100 nm in size. Selected-area electron diffraction (SAED) pattern analysis (inset in Figure 4a) confirmed that the cubic precipitates were NiAl phase. Figure 4b shows a TEM image of the intertexture structure. The intertexture structure consisted of two alternating plate-like phases connected to each other, with the dark region (matrix) having a width of 80–100 nm and the light region approximately 50 nm wide. Combined with XRD analysis results (Figure 3), the matrix was identified as bcc ferrite phase, while the narrower plate-like phase was NiAl phase. The SAED pattern (inset in Figure 4b) demonstrated that the intertexture region consisted of bcc ferrite phase and NiAl intermetallic compound, with the orientation relationship between NiAl phase and ferrite phase ($\alpha\text{-Fe}(\text{Ni}, \text{Cr})$) being $[001]\beta//[001]\alpha$, $(110)\beta//(110)\alpha$, maintaining a coherent or semi-coherent relationship between the two phases. Figure 4c shows a TEM image of the transition region between cubic precipitates and intertexture structure. No distinct interface was observed between the two microstructural regions.

2.2 Microstructural Evolution Mechanism The present experiment involved many reacting elements, making analysis of the FeNiCrAl quaternary alloy system complex. However, the existing FeNiAl ternary alloy system is similar to the FeNiCrAl system and can be used as a starting point for analysis. The binding force between Cr and Fe is much greater than that between Cr and NiAl phase [7], so Cr preferentially combines with Fe to form the α -Fe(Ni, Cr) ferrite phase.

According to the FeNiAl ternary phase diagram at 750 °C [Figure 750: see original paper] (horizontal and vertical cross-sections) proposed by Bradley [16–18], α_1 represents the disordered bcc phase, α_2 represents the ordered NiAl superstructure phase, and γ represents the austenite phase. In the thermite compositions used in this work, the atomic ratio of Fe to Ni was maintained at approximately 5:2. As Al content increased, the composition point of the alloy in the phase diagram changed accordingly. When Al content in the thermite did not exceed 25.4%, the composition point was located in the γ phase region of the phase diagram, and the main constituent phase of the alloy was austenite. In the thermite reaction, Al was insufficient while oxides were in excess. Low Al content prevented complete reduction of metal elements from various oxides, and most Al separated from the alloy as Al_2O_3 slag.

As Al content in the thermite continued to increase, the alloy composition point entered the two-phase coexistence region of α_1 and α_2 in the phase diagram, corresponding to the region where α -Fe(Ni, Cr) matrix and NiAl phase coexisted in this experiment. At this stage, Fe, Ni, and Cr existed in bcc form, while the B2-structured NiAl phase was coherent with bcc α -Fe(Ni, Cr). The low interfacial energy allowed extensive precipitation, achieving coherent precipitation strengthening.

When Al content continued to increase, the shape of NiAl phase observed in this experiment changed from granular to intertexture. This intertexture structure first began to form at grain boundaries. The intertexture structure is very similar to typical spinodal decomposition microstructures (such as the spinodal structure of $\text{Fe}_{30}\text{Ni}_{20}\text{Mn}_{25}\text{Al}_{25}$ [19]) but significantly different from microstructures formed through nucleation and growth processes. The region composed of α -Fe(Ni, Cr) + NiAl two phases represents a miscibility gap, indicating the immiscible region of the two phases. The existence of a miscibility gap in the system is a prerequisite for spinodal decomposition. Therefore, it can be inferred that the formation mechanism of this intertexture structure is spinodal decomposition.

According to Cahn's theory [20–22], when inflection points appear in the composition-free energy curve of a system, uphill diffusion occurs within the inflection region, forming two types of solute-enriched and solute-depleted zones that interconnect to form a network structure. During spinodal decomposition, although the new phase and parent phase maintain a coherent relationship, elastic strain arises between them due to differences in atomic radii of solute and solvent atoms. Since the elasticity of the alloy itself is anisotropic, second-phase

particles after spinodal decomposition tend to grow preferentially and rapidly along crystallographic directions with lower elastic strain resistance to reduce system free energy, resulting in a periodic network structure with perpendicular alignment between the two phases—namely, the intertexture structure.

Based on previous research results [23], it is believed that the spinodal decomposition in this experiment occurred in the liquid phase. In other words, enrichment of Fe and Cr atoms and Ni and Al atoms already existed in the metallic melt while still in the liquid state. Liquid-phase spinodal decomposition was first observed in oxide glasses [24], and recent experimental evidence indicates that liquid-phase separation in alloys occurs in deeply undercooled melts [25–27]. Under deep undercooling conditions, melt viscosity increases while the diffusion coefficient decreases, making liquid-phase separation possible in metals. In this experiment, separation of Al_2O_3 slag from the melt purified the melt and created conditions for deep undercooling. Simultaneously, the extremely fast cooling rate of the melt also made liquid-phase spinodal decomposition possible. When Al content in the thermite was between 27.8% and 30.2%, the lower solidification point at grain boundaries combined with the extremely fast cooling rate of the melt resulted in higher undercooling at grain boundaries, causing the intertexture structure to appear first at grain boundaries. As Al content further increased, liquid-phase spinodal decomposition could satisfy better thermodynamic and kinetic conditions, allowing the intertexture structure to spread throughout entire grains.

When TiO_2 gel was added to the thermite used in this work, numerous dispersedly distributed nanoscale Al_2O_3 particles were found in the synthesized alloy, and these nanoscale Al_2O_3 particles coexisted with NiAl intermetallic compounds [23]. Since nanoscale Al_2O_3 particles can only move in the liquid melt, if spinodal decomposition occurred in the solid phase, the nanoscale Al_2O_3 particles should be uniformly distributed throughout the microstructure. Therefore, it is believed that before alloy solidification, two types of element-enriched zones—Fe, Cr and Ni, Al—already existed. Al_2O_3 particles that precipitated first moved to Ni, Al element-enriched zones with lower interfacial energy due to interfacial energy and Brownian motion. This phenomenon provides strong evidence that spinodal decomposition in this experiment occurred in the liquid phase.

This work also preliminarily investigated the dimensional stability of NiAl phase during high-temperature aging. Figure 5 [Figure 5: see original paper] compares the microstructure of the alloy without aging to those aged at 500, 700, and 900 °C for 100 min. The alloy still exhibited a relatively clear intertexture structure after aging. NiAl phase size was between 60–80 nm, showing some growth compared to the unaged alloy (50–60 nm). Taillard et al. [28] found that when NiAl phase size is less than 300 nm, it can maintain a coherent or semi-coherent relationship with the matrix. Based on this analysis, under the experimental conditions of this work, NiAl phase can still maintain good coherent relationship with the ferrite matrix. More detailed studies on microstructural stability are

ongoing.

2.3 Mechanical Properties Figure 6 [Figure 6: see original paper] shows the tensile stress-strain curves of alloys with varying Al content in the thermite. The tensile strength of the alloys first increased and then decreased with increasing Al content, reaching a maximum of 640.87 MPa at 26.6% Al content. When Al content further increased, tensile strength decreased rapidly.

Figure 7 [Figure 7: see original paper] shows the variation trend of tensile strength and elongation after fracture with Al content in the thermite. Elongation after fracture consistently decreased with increasing Al content, reaching 25.5% at 24.2% Al content but only 1.7% at 29.0% Al content.

Fracture morphologies of alloy tensile specimens are shown in Figure 8 [Figure 8: see original paper]. When Al content in the thermite was 24.2%, the fracture consisted of numerous fine dimples, indicating ductile fracture (Figures 8a and 8b). At 26.6% Al content, the fracture consisted of numerous dimples and river-pattern features characteristic of cleavage (Figures 8c and 8d). Combined with the elongation after fracture greater than 5% at this composition, the fracture mechanism was still ductile. At 29.0% Al content, the fracture showed a stepped microstructure (Figures 8e and 8f), indicating obvious brittle fracture.

When Al content in the thermite was low, the synthesized alloy consisted of fcc austenite (γ -Fe(Ni, Cr)) without NiAl precipitates, exhibiting good ductility and toughness similar to austenitic stainless steel. When the alloy consisted of ferrite, numerous fine NiAl particle reinforcements precipitated, significantly improving alloy strength through precipitation strengthening. However, the appearance of particle reinforcements slightly reduced alloy ductility and toughness. When the volume fraction of NiAl reinforcement further increased and formed an intertexture structure, alloy brittleness increased significantly. This is because NiAl intermetallic compounds are brittle phases at room temperature. When the volume fraction of brittle NiAl phase increased to nearly 50% and interconnected into parallel plates, cracks could easily propagate rapidly along the brittle NiAl phase once initiated, increasing alloy brittleness. Additionally, when Al content in the thermite was high, the synthesized alloy had large grain sizes of 20–30 μm , which was another reason for the alloy's brittleness.

Relevant literature [29] reports that the room-temperature tensile strength of heat-resistant austenitic stainless steel AISI 304 (containing 18% Cr, 8% Ni) is 585 MPa, that of heat-resistant ferritic stainless steel AISI 430 (containing 16–18% Cr) is 539 MPa, and that of corrosion-resistant high-temperature alloy Alloy 800 (containing 21% Cr, 32.5% Ni) is 600 MPa. Teng et al. [30] studied the room-temperature ductility of NiAl-phase-strengthened FeNiCrAl alloys (containing 10% Cr, 10% Ni). Three-point bending test results showed that when the Al mass fraction in the prepared alloy reached 5% or higher, room-temperature elongation was less than 2%. In this work, Fe(Ni, Cr)/NiAl alloys prepared by thermite synthesis achieved a room-temperature tensile strength

of 640.87 MPa with 11.1% elongation when the thermite contained 26.6% Al. Compared with conventional heat-resistant steels, the strength was somewhat improved while the elongation was significantly higher than that of FeNiCrAl alloys strengthened by aged NiAl precipitates.

Conclusions

1. When Al content in the thermite was low, the main constituent phase of the alloy was austenite. As Al content increased, the main constituent phase transformed from austenite to ferrite, accompanied by precipitation of granular NiAl phase. With further increase in Al content, the granular NiAl phase was gradually replaced by an intertexture structure.
2. The intertexture structure consists of α -Fe(Ni, Cr) alloy and plate-like NiAl precipitates. The mechanism for producing the intertexture structure is spinodal decomposition in the liquid phase during cooling.
3. As Al content in the thermite increased, the elongation after fracture of the alloy decreased, reaching 25.5% at 24.2% Al content but only 1.7% at 29.0% Al content. Meanwhile, tensile strength first increased then decreased. The maximum tensile strength of 640.87 MPa was achieved when the thermite contained 26.6% Al.

References

- [1] Masuyama F. *ISIJ Int*, 2001; 41: 612
- [2] Calderon H, Fine M E. *Mater Sci Eng*, 1984; 63: 197
- [3] Pearson W B. *A Handbook of Lattice Spacings and Structures of Metals and Alloys*. Oxford: Pergamon Press, 1958: 347
- [4] Stallybrass C, Schneider A, Sauthoff G. *Intermetallics*, 2005; 13:
- [5] Sudbrack C K, Yoon K E, Noebe R D, Seidman D N. *Acta Mater*, 2006; 54: 3199
- [6] Calderon H A, Fine M E, Weertman J R. *Metall Trans*, 1988; 19A:
- [7] Hao S M, Ishida K, Nishizawa T. *Metall Trans*, 1985; 16A: 179
- [8] Stallybrass C, Sauthoff G. *Mater Sci Eng*, 2004; A387: 985
- [9] Vo N Q, Liebscher C H, Rawlings M J, Asta M, Dunand D C. *Acta Mater*, 2014; 71: 89
- [10] Bradley A J, Taylor A. *Proc R Soc London*, 1938; 166(A926): 353
- [11] Yin S. *Combustion Synthesis*. Beijing: Metallurgical Industry Press, 2004: 1
- [12] Borovinskaya I P. *Pure Appl Chem*, 1992; 64: 919
- [13] Yukhvid V I. *Pure Appl Chem*, 1992; 64: 977
- [14] Fu Z Y. *Acta Mater Comp Sin*, 2000; 17(1): 5
- [15] Hao S M, Takayama T, Ishida K, Nishizawa T. *Metall Trans*, 1984; 15A: 1819
- [16] Bradley A J. *J Iron Steel Inst*, 1949; 163: 19
- [17] Bradley A J. *J Iron Steel Inst*, 1951; 168: 233

- [18] Bradley A J. J Iron Steel Inst, 1952; 171: 41
- [19] Hanna J A, Baker I, Wittmann M W, Munroe P R. J Mater Res, 2005; 20: 791
- [20] Cahn J W. Acta Metall, 1961; 9: 795
- [21] Cahn J W. Acta Metall, 1962; 10: 179
- [22] Cahn J W. Acta Metall, 1962; 10: 907
- [23] Xi W, Peng R L, Wu W, Li N, Wang S, Johansson S. J Mater Sci, 2012; 47: 3585
- [24] Zhang C Q, Yao K F. Acta Metall Sin, 2006; 42: 870
- [25] Ma N G, Kui H W. China Mech Eng, 2000; 11: 1298
- [26] Lee K L, Kui H W. J Mater Res, 1999; 14: 3653
- [27] Yuen C W, Lee K L, Kui H W. J Mater Res, 1997; 12: 314
- [28] Taillard R, Pineau A, Thomas B J. Mater Sci Eng, 1982; 54: 209
- [29] Rothman M F. High-Temperature Property Data: Ferrous Alloys. Metals Park, OH: ASM International, 1987: 250
- [30] Teng Z K, Liu C T, Ghosh G, Liaw P K, Fine M E. Intermetallics, 2010; 18: 1437

Note: Figure translations are in progress. See original paper for figures.

Source: ChinaXiv –Machine translation. Verify with original.